© 2020. Published by The Company of Biologists Ltd | Journal of Cell Science (2020) 133, jcs248864. doi:10.1242/jcs.248864

RESEARCH ARTICLE

CD301 mediates fusion in IL-4-driven multinucleated giant cell formation

Patricia J. Brooks[1,2], Yongqiang Wang[1], Marco A. Magalhaes[1], Michael Glogauer[1,2] and Christopher A. McCulloch[1,*]

ABSTRACT

Multinucleated giant cells (MGCs) are prominent in foreign body granulomas, infectious and inflammatory processes, and auto-immune, neoplastic and genetic disorders, but the molecular determinants that specify the formation and function of these cells are not defined. Here, using tandem mass tag-mass spectrometry, we identified a differentially upregulated protein, C-type lectin domain family 10 member (herein denoted CD301, also known as CLEC10A), that was strongly upregulated in mouse RAW264.7 macrophages and primary murine macrophages undergoing interleukin (IL-4)-induced MGC formation. CD301$^+$ MGCs were identified in biopsy specimens of human inflammatory lesions. Function-inhibiting CD301 antibodies or CRISPR/Cas9 deletion of the two mouse CD301 genes (Mgl1 and Mgl2) inhibited IL-4-induced binding of N-acetylgalactosamine-coated beads by 4-fold and reduced MGC formation by 2.3-fold (P<0.05). IL-4-driven fusion and MGC formation were restored by re-expression of CD301 in the knockout cells. We conclude that in monocytes, IL-4 increases CD301 expression, which mediates intercellular adhesion and fusion processes that are required for the formation of MGCs.

This article has an associated First Person interview with the first author of the paper.

KEY WORDS: IL-4, Macrophage, Monocyte, Inflammation, Mass spectrometry, Foreign body giant cells

INTRODUCTION

Multinucleated giant cells (MGCs) are polykaryons of monocytic origin that are spatially associated with foreign bodies and are seen in infectious, auto-immune, neoplastic and genetic disorders (Kumar et al., 2015). MGCs are morphologically similar despite their occurrence in lesions of different pathogeneses, and arise from the fusion of discrete macrophage subtypes in pathological lesions (Takahashi et al., 1988). Classically activated M1 macrophages are associated with inflammatory processes, whereas alternatively activated M2 macrophages are associated with the resolution of inflammation (Mosser and Edwards, 2008), and characteristically produce ornithines and polyamines through the arginase pathway (MacMicking et al., 1997; Mills et al., 2000). M2 macrophages are further subdivided into various subtypes (M2a, b and c). The generation of one of these subtypes, M2a cells, is promoted by the pro-inflammatory cytokines, IL-4 or IL-13 (Lu et al., 2013).

The formation of MGCs requires cell fusion, which involves the migration of macrophages towards one another and their expression of fusogens that enable cell membrane approximation. This process requires lowering the energy barrier between lipid bilayers of approximating cells (Helming and Gordon, 2009). Currently, the characterization of specific MGC subtypes by histological analysis is challenging, as the molecular determinants and fusogens that specify their formation and function are not defined.

The formation of foreign body giant cells is thought to be regulated by lectins, which detect and bind to glycans expressed by microorganisms (Denda-Nagai et al., 2010; Zelensky and Gready, 2005). Lectins play a role in the activation of the immune system through antigen presentation and cell adhesion. Inhibition of the lectin receptor CD206 (a mannose receptor also known as MRC1), inhibits the formation of foreign body giant cells but does not entirely block fusion (McNally and Anderson, 1995), indicating that other fusogens play central roles in mediating fusion processes. Another, less well-known lectin receptor, macrophage N-acetyl-galactosamine-specific lectin (Mgl/CD301, also known as CLEC10A), which has two murine variants (CD301a/Mgl1 and CD301b/Mgl2), is expressed by macrophages and dendritic cells (Denda-Nagai et al., 2002). Although CD301 is thought to play a role in immune response signaling involving T-cells, its involvement in MGC formation has not yet been described (Denda-Nagai et al., 2010).

Identification of the molecules involved in the formation of MGCs from various monocyte- and macrophage-derived precursors could help to define the role of these cells in MGC-associated diseases, assist in elucidating their pathogeneses, and serve as potential targets for drug discovery. Here, we show that in mouse and human-derived monocytes, the differentially expressed transmembrane protein, CD301, is important for the formation of MGCs induced by IL-4, and that CD301 is expressed in MGC-containing human lesions.

RESULTS

Upregulated proteins in macrophages undergoing fusion

We quantified the formation of MGCs from primary mouse bone marrow monocytes that were activated to become pre-osteoclasts from M1 or M2 macrophages. All nuclei were counted. In those cells with three or more nuclei, we considered that the cell had undergone fusion. The total number of cells that had undergone fusion events (i.e. with three or more nuclei) were expressed as a percentage of the overall nuclear counts (Fig. 1A). The experimental conditions that most effectively promoted cell fusion included RANKL (also known as TNFSF11), IL-1β, IL-4 and TNF, which were then selected for further investigation using tandem mass tag-mass spectrometry (TMT-MS).

Total cell lysates isolated after 5 days of treatment were tagged with stable isotopic labels for analysis by TMT-MS (Table 1).

[1]Faculty of Dentistry, University of Toronto, Toronto, Ontario M5G 1G6, Canada. [2]Department of Dental Oncology & Maxillofacial Prosthetics, Princess Margaret Cancer Centre, Toronto, Ontario M5G 2C1, Canada.

*Author for correspondence (christopher.mcculloch@utoronto.ca)

C.A.M., 0000-0002-3535-8593

Handling Editor: Daniel Billadeau
Received 14 May 2020; Accepted 9 November 2020

Journal of Cell Science (2020) 133, jcs248864. doi:10.1242/jcs.248864

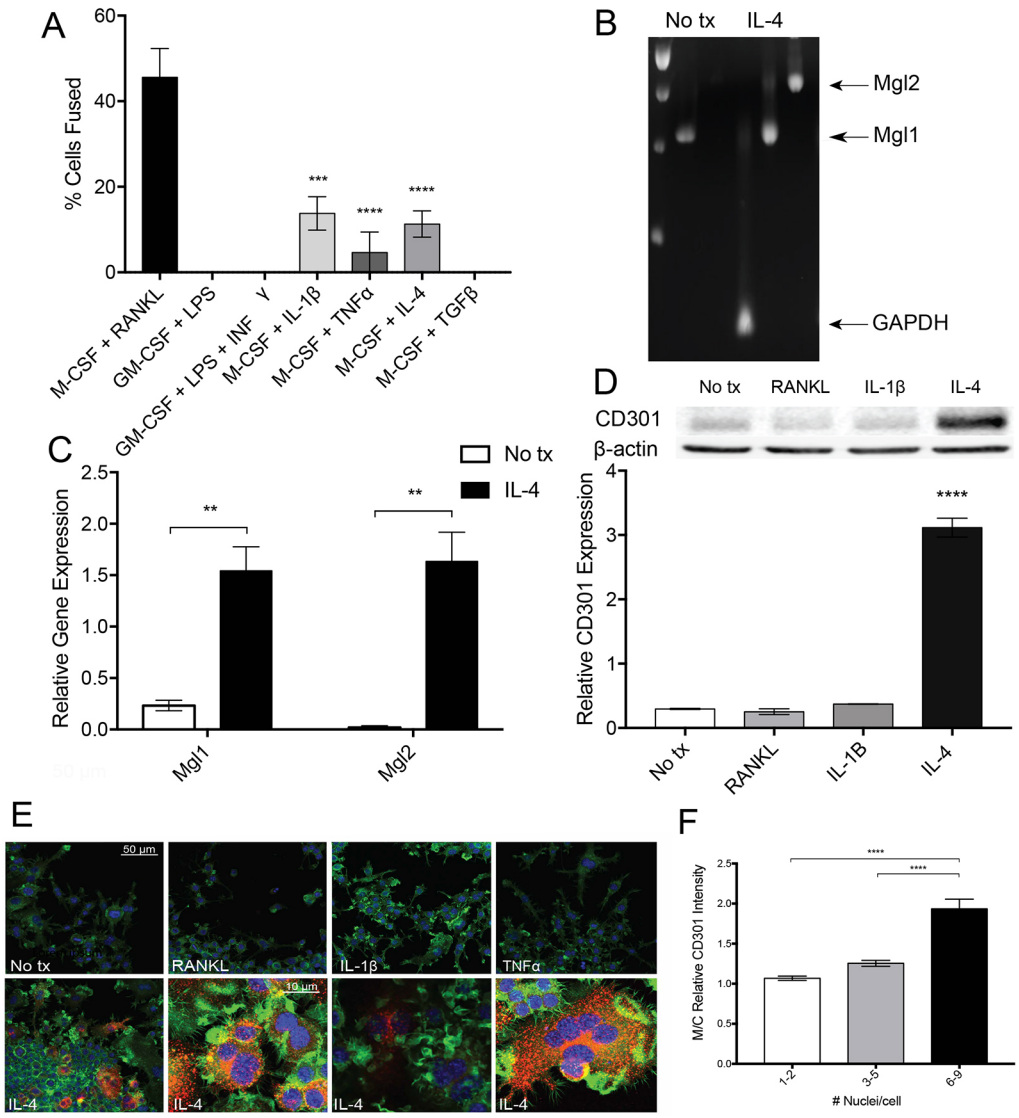

Fig. 1. CD301a and CD301b expression in IL-4-treated RAW264.7 cells. (A) Mouse primary bone marrow monocytes were treated with various cytokine combinations to mediate MGC formation. The percentage of nuclei that underwent fusion events (three or more nuclei per cell) were expressed as a percentage of the overall number of cells. (B,C) RT-PCR and qRT-PCR were performed to assess IL-4-induced *CD301a* (*Mgl1*) and *CD301b* (*Mgl2*) expression using total cell lysate from RAW264.7 cells after 3 days of no treatment or IL-4, standardized to the expression of *GAPDH* (No tx, no treatment to cells). (D) Immunoblotting of total cell lysates in RAW264.7 cells treated with various cytokines for 3 days. In these experiments the immunoblotting antibody detects mouse isoforms of Mgl1 and Mgl2. (E) RAW264.7 cells were treated with various cytokines for 4 days followed by fixation and immunofluorescence staining for CD301 (red), followed by phalloidin (green) and nuclear staining (blue, DAPI). Imaging was performed using a confocal microscope. Scale bars: 50 µm (first five panels); 10 µm (last three panels). (F) Fluorescence intensity measurements were obtained in regions of interest (ROIs) in each IL-4-treated cell expressing CD301. Rectangular ROIs were created along the membrane and cytoplasm, and the intensity of the membrane was divided by that of the cytoplasm. The number of nuclei in each cell was also counted and the relative mean of CD301 intensity was plotted against the number of nuclei per cell. Data are mean±s.e.m. $^{**}P<0.01$, $^{***}P<0.001$, $^{****}P<0.0001$. For each analysis, at least three separate experiments were conducted using four separate cultures.

Proteins that were upregulated or downregulated by a $\log_2$ fold change of more than 0.5 or less than −0.5 were included in the analysis. The protein MCG21506 (CD301b or Mgl2) showed markedly increased abundance after IL-4 treatment (average increased $\log_2$ fold change of 1.0), and was chosen for subsequent and more detailed analysis because of its unexpected expression. Furthermore, we considered that if CD301 was enriched at sites adjacent to the plasma membrane, it may be involved in membrane fusion processes.

We examined Mgl1 and Mgl2 mRNA expression in RAW264.7 cells using RT-PCR and qRT-PCR. *Mgl1* was constitutively expressed and was increased eightfold by IL-4 treatment; *Mgl2* expression was only detectable after IL-4 treatment (Fig. 1B,C). Cells that were treated with vehicle only (i.e. none of the cytokines, IL-1, RANKL and TNF) showed no *Mgl2* expression. There was also no change of basal *Mgl1* levels when compared to cells without cytokine treatment (data not shown). We confirmed that these patterns of *Mgl1* and *Mgl2* mRNA expression were reflected in the measurements of Mgl1 and Mgl2 protein levels by immunoblotting (Fig. 1D), in which the antibody detects Mgl1 and Mgl2 (hereafter designated as CD301).

Localization

Immunolocalization studies showed that mouse CD301 (both isoforms) was expressed in RAW264.7 cells, but only after IL-4 treatment (Fig. 1E). When expressed, CD301 was particularly

Journal of Cell Science (2020) 133, jcs248864. doi:10.1242/jcs.248864

Table 1. Probability scores of proteins expressed by RAW264.7 cells identified by TMT-MS upon treatment with fusogenic cytokines

Identified protein	Molecular mass (kDa)	Accession number	Peptide count	Probability score (log_2 fold)									
				Control		RANKL		IL-1β		TNF		IL-4	
				1	2	1	2	1	2	1	2	1	2
Aldose reductase	36	ALDR	8	0.0	0.0	1.3	1.2	0.0	0.1	0.0	−0.1	−0.2	−0.2
Aminoacylase-1	46	ACY1	25	0.1	−0.1	0.7	0.7	0.1	0.3	0.1	0.1	0.0	0.0
AMP deaminase 3	95	A2AE27	12	0.1	−0.1	0.7	0.7	0.4	0.4	0.3	0.2	0.1	0.1
Annexin A3	36	ANXA3	17	0.0	0.0	−0.6	−0.6	−0.2	−0.3	−0.1	0.0	0.1	0.2
Arginase-1	35	ARG1	2	0.0	0.0	−0.4	−0.1	0.0	−0.2	0.0	−0.1	0.9	0.8
ATP-binding cassette sub-family D	63	A0A0G2JDI9	3	0.2	−0.2	−0.6	−0.6	−0.5	−0.3	0.0	0.0	−0.3	−0.4
CapZ-interacting protein	44	CPZIP	3	0.1	−0.1	−0.7	−0.7	−0.2	−0.1	0.0	−0.2	−0.1	−0.5
Carbonic anhydrase 2	29	CAH2	9	0.0	0.0	1.4	1.2	0.3	0.3	0.0	0.0	−0.1	−0.1
Cathepsin K	37	CATK	5	0.0	0.0	1.3	1.6	0.2	0.4	0.1	0.3	0.1	0.4
Clk2-Scamp3 protein	89	B2M0S2	5	0.0	0.0	−0.2	0.0	0.6	0.5	0.2	0.1	0.0	0.1
Cytochrome b-245 heavy chain	65	CY24B	15	0.0	0.0	−0.6	−0.7	−0.1	−0.1	−0.1	0.0	−0.2	−0.2
Death-associated protein 1	9	A0A087WR57	5	−0.1	0.0	1.0	0.8	0.3	0.3	0.0	0.1	0.2	0.1
EH domain-containing protein 1	61	EHD1	19	0.0	0.0	0.5	0.6	0.3	0.3	0.1	0.1	−0.2	−0.2
Ena/VASP-like protein	43	E9PVP4	2	0.0	0.0	−1.8	−1.0	−0.4	−0.7	−0.1	−0.1	0.0	−0.1
Fatty acid desaturase 2	52	FADS2	2	0.0	0.0	−1.2	−1.8	−0.2	−0.1	−0.2	0.3	−0.1	−0.4
FERM domain-containing protein 48	118	FRM4B	2	−0.1	0.1	−1.0	−1.4	−0.1	0.5	0.5	0.4	0.4	0.3
Formin-1	164	FMN1	2	0.4	−0.3	0.9	1.3	1.4	1.6	0.8	1.2	0.6	1.0
Guanine deaminase	51	QUAD	5	0.0	−0.1	0.0	−0.1	0.3	0.3	0.1	0.1	0.8	0.9
H2-Ab1 protein	30	Q95I79	2	0.1	−0.1	−0.1	−0.2	0.1	−0.2	−0.2	0.0	1.4	1.7
Heat shock 70 kDa protein 4L	94	HS74L	16	0.0	0.0	0.6	0.6	0.2	0.3	0.0	0.0	−0.1	−0.1
Hematopoietic prostaglandin D synthase	23	HPGDS	2	0.1	−0.1	−0.8	−0.8	−0.4	−0.4	0.0	−0.1	−0.3	−0.3
High mobility group protein HMG-I	12	HMGA1	5	0.0	0.0	0.9	0.9	0.2	0.2	0.0	0.0	0.1	0.0
Kinectin	146	A0A087WQQ5	16	0.0	0.0	0.6	0.7	0.2	0.2	0.1	0.1	0.1	0.2
MCG21506/CD301b	44	A9XX86	3	−0.1	0.1	0.1	0.2	0.3	0.1	0.2	0.2	0.9	1.1
Myeloid cell nuclear differentiation antigen-like protein	61	MNDAL	4	0.0	0.0	−0.6	−0.6	−0.1	−0.3	0.1	0.0	−0.1	−0.1
Peptidyl–prolyl-cis-trans isomerase FKBP11	22	FKB11	2	0.1	−0.1	0.8	1.1	0.3	0.6	0.2	0.3	0.2	0.2
Protein Krt78	112	E9Q0F0	2	−0.2	0.2	0.5	0.4	1.4	0.6	0.1	−0.2	1.1	0.6
Protein Upf2	148	A2AT37	2	0.0	0.0	−0.8	−0.8	0.3	0.0	−0.2	0.1	−0.3	0.2
Sugar phosphate exchanger 2	55	SPX2	2	0.1	0.1	0.8	0.7	0.0	0.0	0.0	−0.1	−0.2	0.0
Superoxide dismutase	25	Q4FJX9	7	0.0	0.0	0.4	0.6	0.0	0.0	−0.1	0.0	−0.1	0.0
Tartrate-resistant acid phosphatase type 5	37	PPA5	8	0.1	−0.1	1.4	1.4	0.2	0.5	0.1	0.1	−0.1	0.1
Transcriptional regulator ATRX	279	ATRX	6	0.1	0.0	−0.7	−0.6	−0.3	−0.1	−0.1	0.1	0.0	0.1
Tropomyosin 1, alpha isoform CRA	29	E9Q7Q3	2	0.0	0.0	0.6	0.5	0.3	0.3	0.1	0.1	0.3	0.1
V-type proton ATPase subunit d 2	40	VA0D2	7	0.0	0.0	0.8	0.7	0.1	0.3	0.0	0.1	0.1	0.1
Vitronectin	55	VTNC	2	0.1	0.1	0.8	0.9	0.2	0.5	0.3	0.2	0.0	0.1

The data in two separate experiments are shown (1 and 2 for each treatment). RAW264.7 cells treated for 5 days with RANKL, IL-1β, TNF, IL-4 or vehicle (control). Scaffold 4.0 was used to compute *P*-values. Proteins that exhibited log_2 fold change greater than 0.5, or less than −0.5, with $P<0.05$ when compared to the control, are tabulated. The peptide counts described here were derived from those counts with a probability of $P<0.05$. The protein of interest, MCG21506/CD301b, is highlighted in bold.

abundant in the cytoplasm near the plasma membrane in cells with multinucleation. We quantified CD301 localization by measuring the fluorescence intensity of CD301 in regions of interest in the cytoplasm and over the plasma membrane, and these data were expressed as a ratio (Fig. 1F). The relative abundance of CD301 staining that localized to the plasma membrane increased nearly twofold when cells with one or two nuclei, or with six to nine nuclei, were compared ($P<0.0001$).

These evaluation methods were deepened using a separate labeling method to examine plasma membrane-localized CD301. We immunostained cells for CD301 and the plasma membrane label fluorescent concanavalin A (see Materials and Methods) to assess the spatial relationship of CD301 with the plasma membrane. In these preparations, CD301 was more obviously localized adjacent to the plasma membrane (before fixation; Fig. 2A) compared with single antibody immunostaining described above. By quantitative analysis, a moderate level of spatial colocalization (Pearson's correlation coefficient) between concanavalin A and CD301 was found in these cell preparations ($r=0.54$ to 0.64 in four different experiments; $P<0.01$). We extended these studies by examining plasma membrane proteins that were isolated by affinity labeling with concanavalin A (Lee et al., 2008). In these preparations, Na^+/K^+-ATPase was used as a plasma membrane marker protein (Fig. 2B). CD301 was expressed only in IL-4-treated cells and by densitometry we found there was 30-fold more CD301 in the plasma membrane fraction compared with the cytosolic fraction.

Effect of CD301 inhibition on glycan-bound bead binding and cell fusion

Purified glycans, Le^X and GalNAc, which are cognate ligands of Mgl1 and Mgl2, respectively, were bound to beads and incubated with IL-4-treated cells, or with IL-4-treated cells that had been pretreated with an inhibiting antibody (designated here as CD301 as it targets mouse Mgl1 and Mgl2 isoforms; Fig. 3A). Differential interference contrast images were overlaid with fluorescence microscopy images to show the location of the beads on the cells. IL-4 treatment increased binding of Le^X and GalNAc beads by threefold and sevenfold, respectively (Fig. 3B). Treatment with the Mgl1/2 inhibitory antibody decreased binding of Le^X and GalNAc beads by 1.5- and fourfold, respectively, when compared to IL-4

Journal of Cell Science (2020) 133, jcs248864. doi:10.1242/jcs.248864

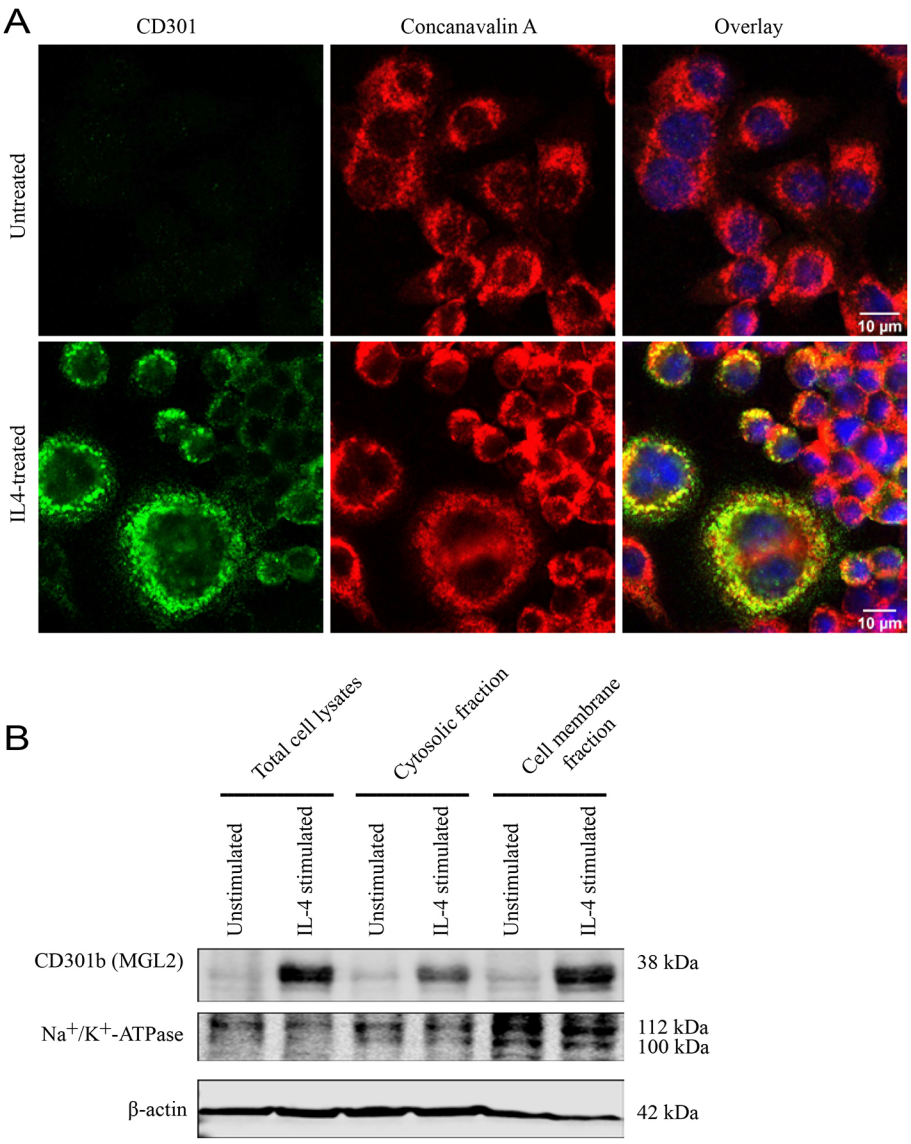

Fig. 2. Immunostaining and immunoblot analyses demonstrate that CD301 is mainly localized to the cell periphery of IL-4 treated cells. (A) RAW264.7 cells were treated with IL-4 (green) for 4 days, labeled with concanavalin A (red), immunostained with CD301 antibody and counterstained with DAPI (blue). Scale bars: 10 µm. (B) Immunoblot analysis showing increased abundance of CD301 in the plasma membrane fraction compared with the cytosolic fraction. In these experiments, RAW264.7 cells were treated with IL-4 for 4 days. Total cell lysates, cytosolic and membrane fractions were separated by SDS-PAGE and analyzed by immunoblotting. For the NaK-ATPase, several bands were detected at ∼110 kDa, which presumably represents the 112 kDa NaK-ATPase. These experiments were repeated three times using separate cultures with similar results.

treatment alone. As the inhibiting antibody blocked Mgl1 and Mgl2 ligand binding, we examined cell fusion after antibody inhibition of CD301 function. Cells were treated with IL-4 for 6 days and then with the Mgl1/2 inhibitory antibody or an isotype control antibody, and the percentage of cells that underwent fusion was determined (Fig. 3C-E). Antibody inhibition reduced by twofold the percentage of IL-4 treated cells that underwent fusion (Fig. 3D). Furthermore, the number of multinucleated cells with three to five nuclei or with more than six nuclei per cell were quantified in the control and antibody inhibition groups. After inhibition of CD301, the number of cells with six or more nuclei per cell was reduced more than 15-fold (from 1.6±0.2 to 0.1±0.1, compared with the control group; P<0.0001; Fig. 3E).

CRISPR CD301 knockout

Mgl1 knockout (KO), Mgl2 KO, and Mgl1/2 double KO (DKO) cells were generated (Fig. S1), and their survival and growth over 5 days was evaluated (Fig. S2). In some experiments, Mgl2 KO or DKO cells were stably transfected with an Mgl2 expression vector. The localization and abundance of CD301 protein expression were examined by immunofluorescence and immunoblotting after IL-4 treatment (Fig. 4A-E). An antibody to CD301 that detects Mgl1 and Mgl2 isoforms was used for immunostaining (designated as Mgl2 in immunoblot). Protein expression was readily visualized in wild-type and Mgl1 KO cells after IL-4 treatment but was not detectable in Mgl2 KO or DKO cells. The immunoblot shows that Mgl2 KO and DKO cells that were transfected with Mgl2 exhibited abundant CD301 staining without IL-4 stimulation, presumably reflecting constitutive activity of the 5′-long-terminal repeat retroviral promoter in the Mgl2 expression vector. Separate measurements of Mgl2 expression after IL-4 treatment were obtained by flow cytometry analysis of wild-type and KO cells after no treatment or IL-4 treatment (Fig. 4F). Mgl2 expression was increased after 4 days of treatment with IL-4, but the KO cells showed no detectable signal, even in the presence of IL-4 (median fluorescence intensity and relative numbers of $Mgl2^+$ cells expressed as percentage of total cell population; Fig. 4G).

Glycan-bead binding and cell fusion in Mgl1/2 KO cells

When wild-type, Mgl1 KO, Mgl2 KO or DKO cells were incubated with glycan-bound beads, there was decreased binding of Le^X beads (more than twofold) in Mgl1 KO and DKO cells compared with wild-type cells and Mgl2 KO cells (Fig. 5A). When these same groups of cells were incubated with GalNAc beads, there was more than fourfold reduced bead binding for Mgl2 KO or DKO cells

Journal of Cell Science (2020) 133, jcs248864. doi:10.1242/jcs.248864

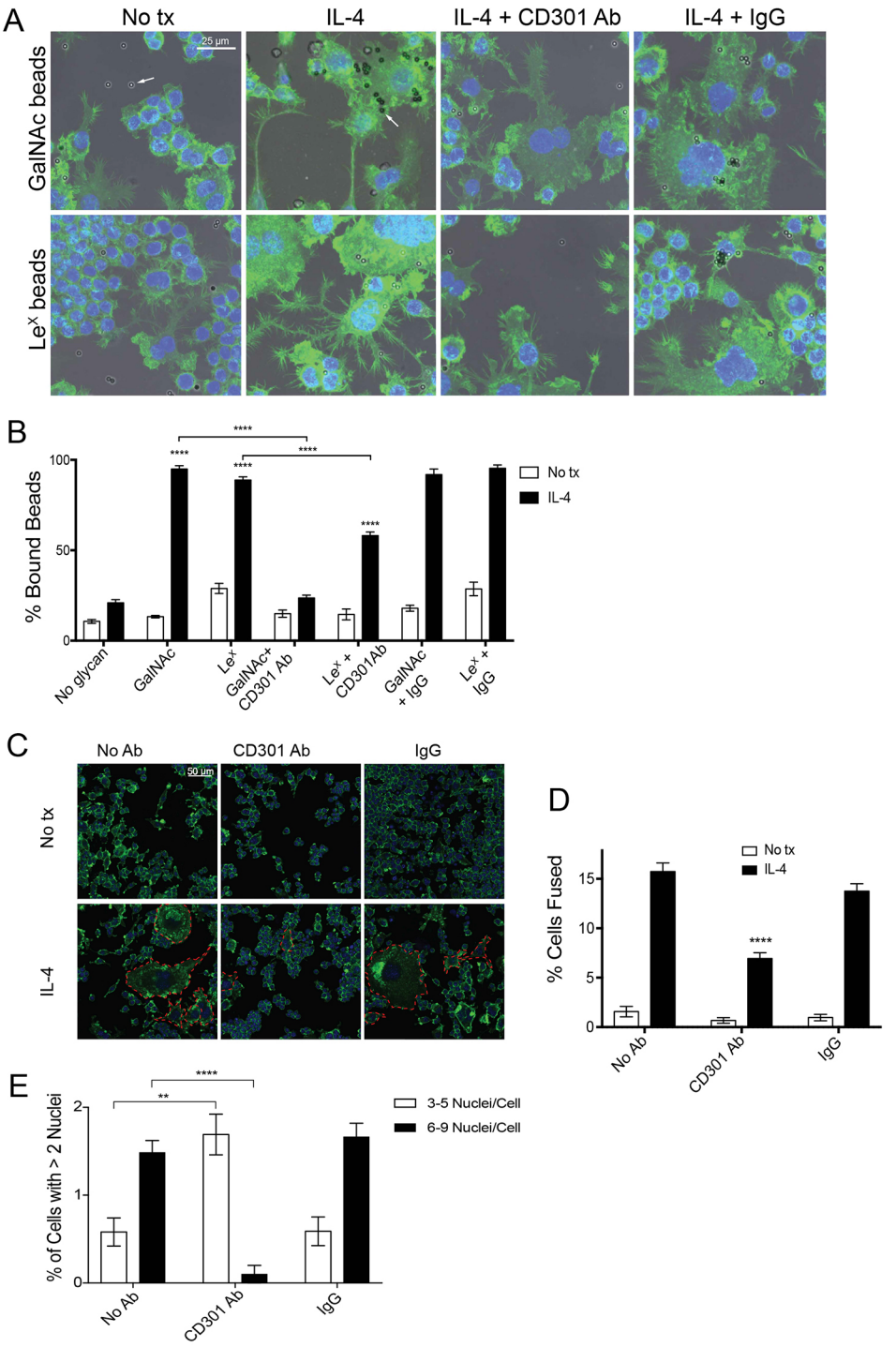

Fig. 3. Glycan-bound bead binding and cell fusion with inhibition. (A) RAW264.7 cells with no treatment (No tx), IL-4 treatment alone, IL-4 with CD301 blocking antibody (CD301 Ab), or IL-4 with an isotype control antibody (IgG), were treated with or without IL-4 for 3 days, then incubated with the antibodies for 1 h, followed by 1 h with GalNAc or LeX-bound beads. Cells were fixed and stained with Alexa Fluor 488 phalloidin (green) and DAPI (blue). The fluorescence and differential interference contrast images have been overlaid, which causes image washout. Arrows indicate bound beads. (B) The total number of beads attached to cell membranes was counted. The number of unbound beads and bound beads were also counted. Data are expressed as a percentage of the overall number of beads. (C) RAW264.7 cells received either no treatment or IL-4 treatment for 6 days with no antibody (No Ab), CD301 antibody or IgG (isotype control antibody). Cells were fixed and stained with Alexa Fluor 488 phalloidin (green) and DAPI (blue). (D) Quantification of the percentage of cells that underwent fusion events. The no antibody-IL-4-treated group was used as the comparison control. In at least 25 high power microscope fields, the total numbers of nuclei were counted for each cell. The percentage of those cells that exhibited multinucleation (i.e. more than two nuclei) was computed. These cells were considered to have undergone fusion. (E) Quantification of number of cells with more than two nuclei per high power field. Data were obtained from analysis of at least 25 high power microscope fields. The data from the groups were divided into multinucleated cells with 3-5 nuclei/cell or cells with 6-9 nuclei/cell. Data are mean±s.e.m. $^{**}P<0.01$, $^{****}P<0.0001$. Scale bars: 25 µm (A); 50 µm (C). All experiments were repeated three or more times on separate days using different cell cultures. Each experiment was comprised of at least three different cultures.

compared with wild-type cells and Mgl1 cells. Collectively, these data show that the binding of glycan beads with their cognate partners was decreased in the expected KO cell groups.

In wild-type and KO cell lines treated with IL-4 (Fig. 5B), cell fusion was decreased by 2.2- and 4.8-fold in Mgl2 KO and DKO cells, respectively, compared with wild-type cells. Notably, there was no detectable reduction of fusion of the KO cells compared with wild-type cells after treatment with RANKL (Fig. S3). The Mgl2 KO cells that were rescued with Mgl2 and the DKO cells that were rescued with Mgl2, exhibited cell fusion with or without IL-4 treatment, and there was no difference in the number of cell fusion events between these groups ($P>0.2$), indicating that Mgl2 expression and not IL-4 treatment per se, promoted cell fusion.

We examined the ability of KO cells to undergo fusion if their proximity to one another was increased. This experiment was conducted by plating cells at three different densities (10^3, 10^4 and 10^5 cells/well). After 6 days of IL-4 treatment, cells were fixed and the number of cells that underwent fusion events was analyzed (Fig. 5C). For wild type and the various KO cell lines, there were no statistically different proportions of fusions at the different plating densities ($P>0.2$). Furthermore, Mgl2 KO and DKO cells all showed statistically different numbers of fusion events compared with wild-type cells at all plating densities ($P<0.0001$).

Journal of Cell Science (2020) 133, jcs248864. doi:10.1242/jcs.248864

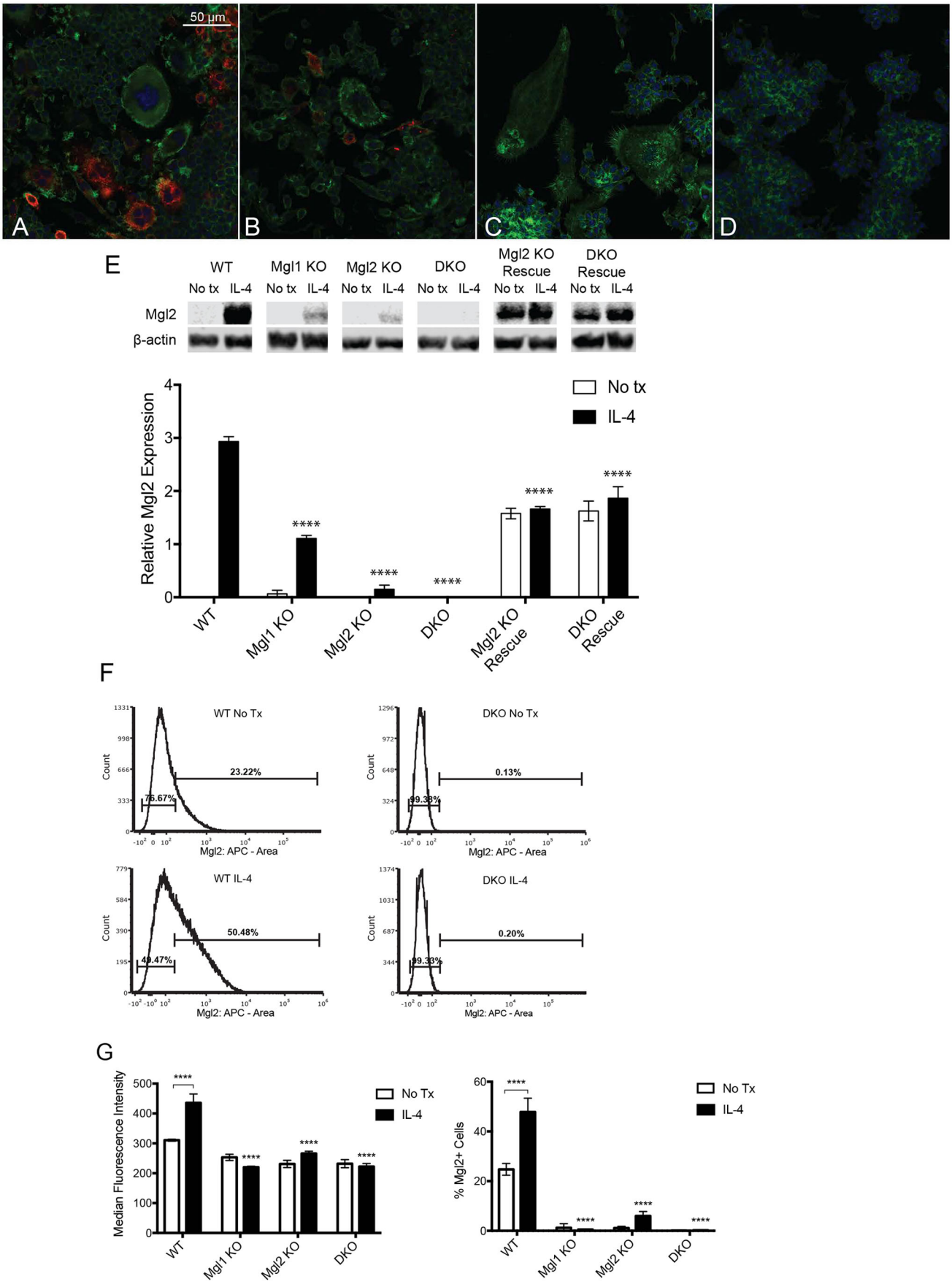

Fig. 4. See next page for legend.

Fig. 4. CD301 expression in CRISPR knockout cells and Mgl2-rescued cells. RAW264.7 wild-type and KO cells were cultured for 4 days with or without IL-4, followed by fixation and immunostaining. (A-D) IL-4-treated cells were immunostained for CD301 (red), followed by Alexa Fluor 488 phalloidin (green) and nuclear staining (DAPI; blue). Scale bar: 50 µm. A shows wild-type cells; B shows Mgl1 KO cells; panel C shows Mgl2 KO cells; and D shows DKO cells. (E) Immunoblotting of total cell lysates in which the CD301 antibody used here detects Mgl1 and Mgl2 isoforms (designated as Mgl2 on blots). B-actin was used as a loading control. The wild-type (WT)-IL-4-treated group was used as the comparison control. The histogram below the immunoblots shows relative blot density for CD301, as adjusted for beta-actin from four different experiments. The data are mean±s.e.m. adjusted blot density. (F) Representative flow cytometric data from single flow cytometry runs for analysis of Mgl2 expression in wild-type and KO RAW264.7 cells that were not treated or treated with IL-4, as indicated. (G) Histograms showing median fluorescence intensity (left) and median percentage of $Mgl2^+$ cells (right), in which the wild-type-IL-4-treated group was used as the comparison control. The data were analyzed from four separate experiments using different cultures for each analysis. The error bars are the inter-quartile ranges. ****P<0.0001. All experiments were repeated on three or more days, using at least three cultures for each day`s experiments.

Human monocytic cell fusion, CD301 expression and MGC formation

THP-1 human monocyte-like cells were treated with pro-fusogenic cytokines to assess the formation of multinucleated cells. Treatment with human macrophage CSF (hM-CSF; also known as CSF1) with IL-4 or RANKL enhanced MGC formation, but no fusion occurred after hM-CSF treatment alone (Fig. 6A,B). CD301 mRNA expression was measured by qRT-PCR (Fig. 6C). The cells all exhibited low basal *CD301* levels but *CD301* expression was increased by nearly fivefold above control levels after treatment with IL-4. THP-1 cells cultured under pro-fusogenic conditions were subjected to different treatments to assess the effects of inhibition or activation of CD301 on cell fusion (Fig. 6D,E). For the activation of CD301, cultures were incubated with N-acetylgalactosamine (GalNAc), a high affinity glycan ligand for human CD301. Recombinant human CD301 (rhCD301) was added to bind glycan partners, in order to inhibit the activation of the cell-bound lectin. In cells treated with IL-4, rhCD301 reduced cell fusion by nearly tenfold compared with controls (P<0.0001). In cultures treated only with hM-CSF, there were no fused cells, but the presence of GalNAc promoted fusion to a level similar to that observed with IL-4 treatment alone. In cells treated with RANKL, there was only a small reduction of the percentage of fused cells in the presence of soluble GalNAc. Furthermore, GalNAc did not inhibit RANKL-driven cell fusion after treatment with rhCD301.

Human sample analysis

We examined whether MGCs in human pathological lesions expressed CD301. Two reactive/reparatory lesions were studied, the central giant cell granuloma (CGCG) and peripheral giant cell granuloma (PGCG). Immunohistochemistry of the two variants of the giant cell granuloma was performed, and showed that CD301 and the transmembrane protein CD68 were highly expressed by cells of the monocytic lineage (Fig. 6E). Mononucleated and multinucleated cells exhibited CD301 staining in both lesions.

DISCUSSION

We used TMT-MS to obtain new insights into the mechanisms of monocytic cell fusion, which led to the discovery of the transmembrane protein Mgl2 and its role in the formation of MGCs in mice. The human variant of CD301 (also called C-type lectin domain family 10 member) is a transmembrane protein in the group of lectin receptors known as C-type lectin receptors, to which the mannose receptor also belongs (a pro-fusogen in osteoclasts) (Zelensky and Gready, 2005). CD301, which is expressed by human dendritic cells and macrophages, and is involved in immune response signaling through interactions with effector T-cells (Higashi et al., 2002; van Vliet et al., 2006), is upregulated by IL-4 and is considered to be a marker of M2 macrophages (Raes et al., 2005). These findings are consistent with our TMT-MS, mRNA, immunostaining and immunoblot data, and the impact of the M2 activator IL-4 and its upregulation of CD301 expression (Raes et al., 2005). Notably, the other variant of the CD301 protein in mice, Mgl1, did not show differential expression, at least as assessed by our threshold for analysis by TMT-MS (i.e. more than 0.5 $\log_2$ fold change between the various cytokine treatments). Mgl1 exhibits different glycan affinity binding profiles than Mgl2, and when knocked out using CRISPR/Cas9, there was no significant difference in the number of IL-4-induced cell fusion events compared with the number in wild type (Singh et al., 2009). Mouse Mgl2 is similar in amino acid sequence and carbohydrate specificity to human CD301 (Denda-Nagai et al., 2010). Correspondingly, we found that deletion of the Mgl2 gene in mouse macrophages led to similar findings with respect to IL-4-mediated cell fusion in human cells.

When we immunostained the two isoforms of CD301 (Mgl1 and Mgl2) in mouse monocytes with a non-isoform-specific antibody, we found that as the number of nuclei increased, CD301 became more localized to the plasma membrane. Furthermore, when another non-isoform-specific antibody was used to block IL-4-induced fusion, there were reduced overall numbers of fusion events. The numbers of cells with six or more nuclei per cell were greatly decreased but the numbers of cells with three to five nuclei were slightly increased. This finding, along with the localization of CD301 to the plasma membrane of larger cells, suggests a role for CD301 in the formation of larger MGCs and in fusion events at later stages of MGC formation. A similar observation was made after inhibition of the mannose receptor in IL-4-driven multinucleation and osteoclast formation (McNally et al., 1996; Morishima et al., 2003). In both of these fusion conditions, the formation of multinucleated cells does occur, but multinucleation occurs to a lesser extent. These parallel findings, which also involve a C-type lectin receptor, support the notion that this type of receptor is involved in later fusion events. Conceivably, another fusion molecule leads to the formation of smaller MGCs. A possible candidate protein that enables early fusion events is the dendritic cell-specific transmembrane protein (Dcstamp), as it is required for the formation of IL-4-driven multinucleation and osteoclastogenesis (Yagi et al., 2005).

In the human monocytic cell line THP-1, we found that CD301 expression was upregulated by IL-4 treatment. With the addition of exogenous recombinant human CD301 to cultures, which reduced the availability of membrane-bound and free glycans, we found that IL-4-induced cell fusion was greatly decreased. This competitive inhibition of cell fusion by the addition of excess CD391 did not occur in RANKL-treated cells. Notably, we observed by qRT-PCR that *CD301* is expressed at moderate levels when cells were treated with hM-CSF alone. When the glycan ligand for CD301 (GalNAc) was added to cells, MGC formation occurred without the need for IL-4, suggesting that constitutive expression levels of CD301 were sufficient to promote cell fusion events, at least to a limited degree. When Mgl2 was re-expressed in the KO mouse cell lines, not only was cell fusion restored, but these cells no longer required IL-4 for cell fusion to occur. Taken together, these results suggest that ligand binding to CD301 (or Mgl2) alone can stimulate monocyte fusion. The experimental interventions that reduced fusion events in these experiments suggest that it is either a lectin-glycan interaction or a

Journal of Cell Science (2020) 133, jcs248864. doi:10.1242/jcs.248864

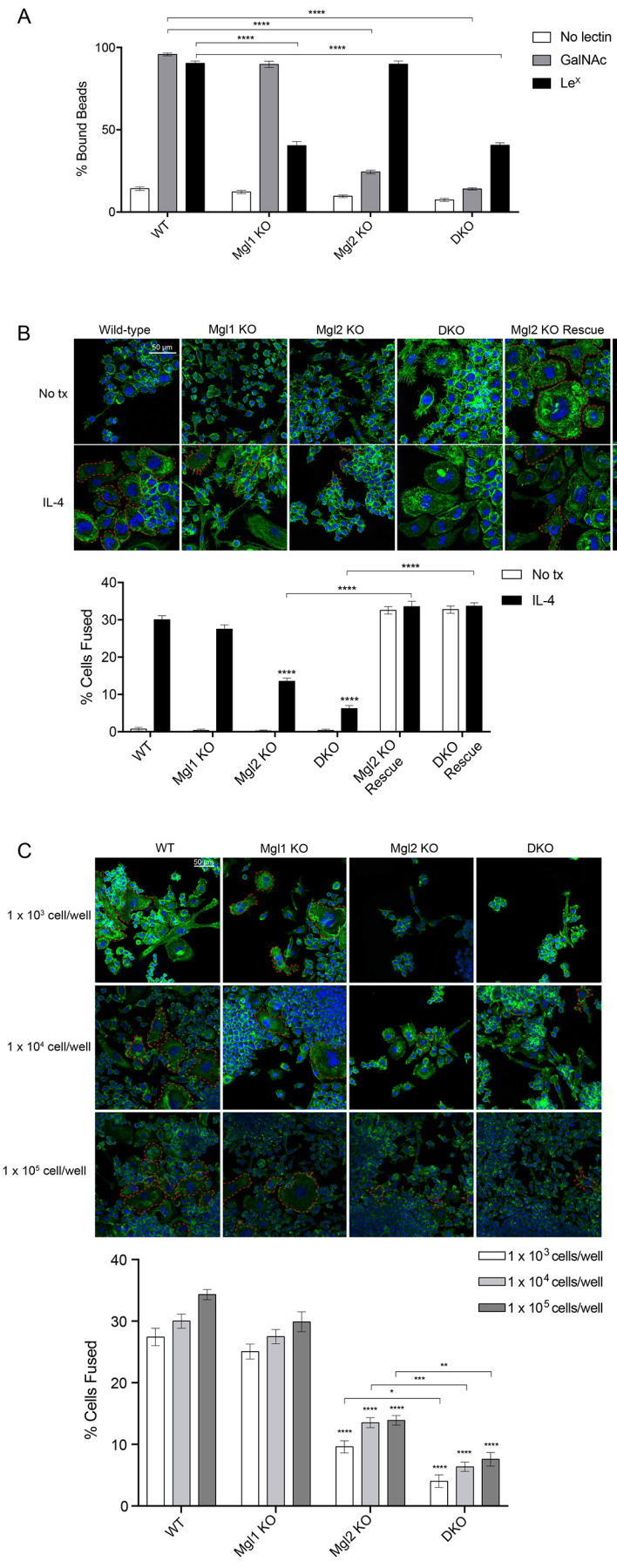

Fig. 5. Glycan-bound bead binding and cell fusion with wild-type and KO cells. (A) wild-type (WT), Mgl1 KO, Mgl2 KO or DKO cells were treated with IL-4 for 3 days, then incubated for 1 h with indicated glycan-bound beads (i.e. GalNAc or Le^X) or beads with no bound glycan as controls. Cells were fixed and stained with Alexa Fluor 488 Phalloidin and DAPI. The percentage of bound beads was estimated from microscopic counts of individual fields from overlaid fluorescence and differential interference contrast images from four separate experiments, each of which evaluated at least 100 cells per field. Using the overlaid images, the total number of beads attached to cell membranes was counted. The number of unbound beads (i.e. not directly in contact with cells) and the bound beads were counted, and for each image field, the number of attached beads was divided by the total number of beads to provide the percentage of bounds beads. Data are mean±s.e.m. of percentage of bound beads. (B) Wild-type, Mgl1 KO, Mgl2 KO, DKO cells KO, Mgl2-rescued Mgl2 KO cells and Mgl2-rescued DKO cells were cultured with and without IL-4 for 6 days. Cells were fixed and stained with Alexa Fluor 488 Phalloidin (green) and DAPI (blue). Quantification of cell fusion was performed as described in Materials and Methods. Fused cells are indicated in the image by red dashes around the periphery of cells. Data are mean±s.e.m. of percentage of fused cells in four microscope fields from four separate experiments conducted on different days. The percentage of fused cells was computed from the number of multinucleated cells (three or more nuclei) divided by the total numbers of cells in each field. (C) Wild-type and KO cells were cultured with IL-4 for 6 days at 10^3, 10^4 and 10^5 cells/well. After 6 days, cells were fixed, stained with Alexa Fluor 488 Phalloidin (green) and DAPI (blue), and quantified as in B. Fused cells are indicated in image by red dashes around the periphery of cells. Wild-type cells at the same plating density were used as the control. Data are mean±s.e.m. *P<0.05; **P<0.01; ***P<0.001; ****P<0.0001. Scale bars: 50 µm. All experiments were repeated on four different days and the repeats within day are indicated above.

Journal of Cell Science (2020) 133, jcs248864. doi:10.1242/jcs.248864

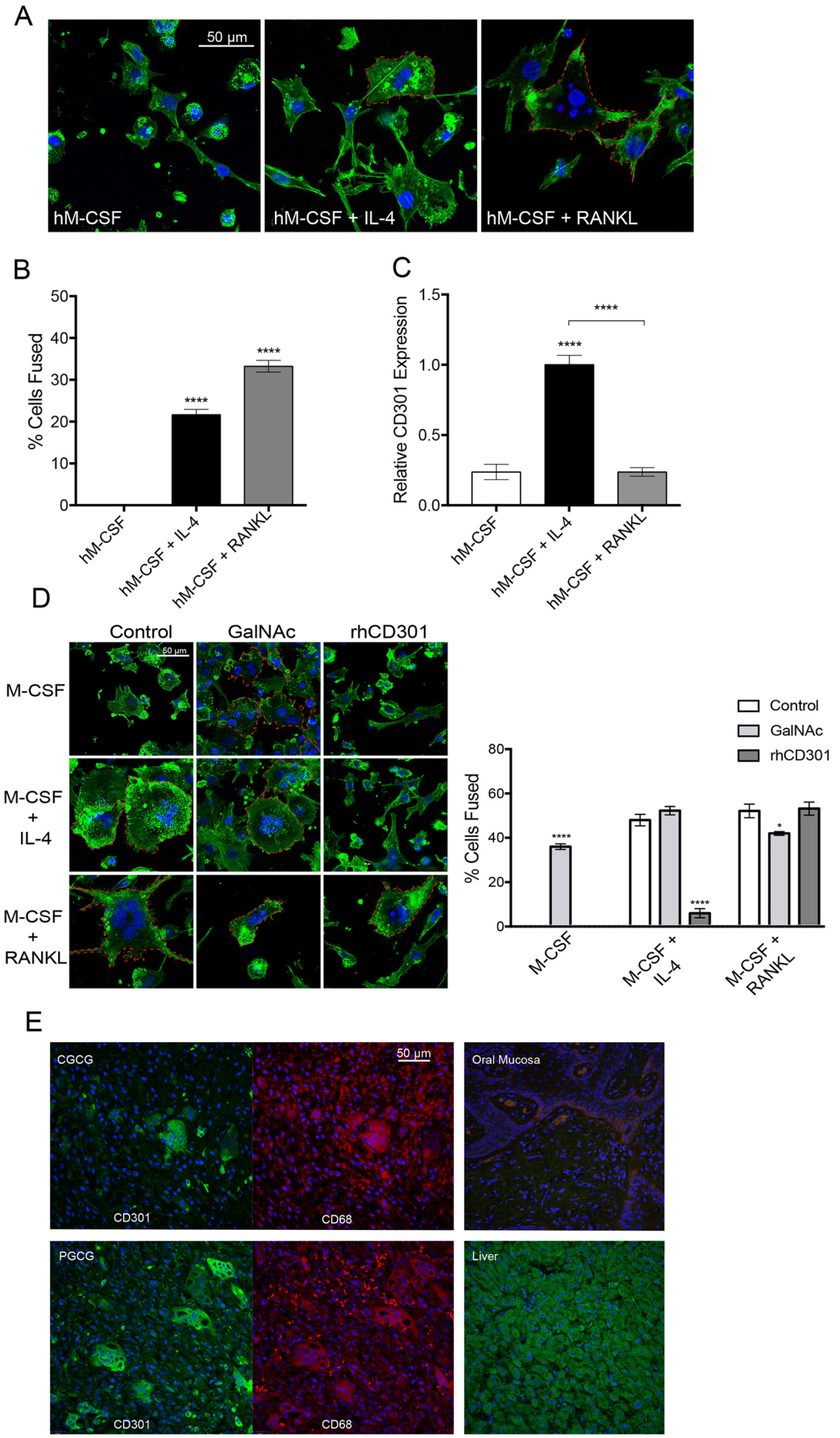

Fig. 6. See next page for legend.

Fig. 6. Cell fusion and CD301 expression after treatment with fusogenic cytokines and in human lesions. (A) THP-1 cells were treated with hM-CSF alone or together with IL-4 or RANKL for 12 days, then fixed, and stained with Alexa Fluor 488 phalloidin (green) and DAPI (blue). (B) Quantification of THP-1 cell fusion, in which the total numbers of nuclei were counted and the percentage of those in multinucleated cells (three or more nuclei) were considered to have undergone fusion. hM-CSF treated cells were used as the comparison control. (C) Total cell RNA was analyzed using qRT-PCR for CD301 expression in cells treated with hM-CSF alone or with IL-4 or RANKL. Results were normalized to GAPDH. (D) Cells received either hM-CSF alone, or hM-CSF with IL-4 or RANKL for 12 days with no other treatment, GalNAc glycan, or recombinant human CD301. Cells were fixed and then stained with Alexa Fluor 488-phalloidin (green) and DAPI (blue). The total number of nuclei in cells prepared as shown in this panel were counted, and the percentage of those cells showing multinucleation (i.e. more than two nuclei; highlighted with red dashes) were considered to have undergone fusion. (E) Immunohistochemical staining of CD301 (green), CD68 (red) and nuclei (blue) in two MGC-containing reactive human lesions of the head and neck. Healthy oral mucosa and liver served as negative and positive controls, respectively. Data are mean±s.e.m. *P<0.05, ****P<0.0001. Scale bars: 50 µm.

CD301-GalNAc interaction that promotes cell fusion. In this context, allosteric activation of CD301 may promote ERK1/2 signaling, which is known to regulate the function of the Arp2/3 complex and to promote actin assembly in nascent lamellipodia (van Vliet et al., 2013). The formation of lamellipodia may facilitate approximation of plasma membranes in adjacent cells after an initial CD301/Mgl2-glycan interaction (Mendoza et al., 2015). As a result of subcortical actin assembly and its integration into protrusion-dependent processes leading to fusion, pores in the plasma membrane are formed, as seen in the fusion of myoblasts, which enables sharing of cytoplasmic contents between fusing (Sens et al., 2010).

Our original goal was to identify a differentially expressed fusogen in MGCs derived from cells with different origins to improve, over the long term, diagnosis of MGC-containing lesions. We found that in the CGCG and the PGCG, mononuclear $CD68^+$ cells and MGCs were stained for CD301. There is a long-standing debate on whether the CGCG and PGCG are only intra- and extra-osseous versions of one another (Gupta et al., 2019; Neville et al., 2016). IL-10, a cytokine released by alternatively activated M2a cells, is a marker of anti-inflammatory macrophages (Wang et al., 2019). IL-10, along with its receptor, is thought to be equally expressed by MGCs of CGCGs and PGCGs (Syrio et al., 2011). In studies of peripheral blood of patients with CGCGs, monocytes showed increased IL-10 expression compared with lymphocytes or with control monocytes, indicating a possible M2b phenotype (Souza et al., 2005). Our findings of CD301-stained mononuclear and multinucleated cells in the PGCG and CGCG lesions supports the notion that these lesions are associated with an M2 macrophage subtype and are involved in reactive/reparative processes.

Although a linkage between M2 macrophages and MGC formation has been described previously (McNally and Anderson, 2011), a role for CD301 in cell fusion leading to MGC formation has not been reported. Previously, it was thought that CD206 is important for foreign body (or IL-4-induced) MGC formation. However, CD206 is also involved in the formation of osteoclasts (RANKL-induced MGC formation) (McNally et al., 1996; Morishima et al., 2003). Our findings from human and mouse cell lines show that CD301 and Mgl2, respectively, are required for the formation of IL-4-induced MGCs, but the formation of osteoclasts was not affected in cells from either species. This finding could be relevant for new diagnostics or therapies. Currently, CD206 is known to be expressed by two different MGC subtypes, whereas CD301 is only expressed by one, thereby providing a possible marker for differentiating between the two subtypes. CD301, also appears to be involved in the formation of MGCs with larger numbers of nuclei, those which may cause the greatest number of issues pathologically to patients. Some current therapeutic approaches have targeted CD206, or RANKL (in the formation of osteoclast-like giant cells), as both of these molecules are important for osteoclast formation (Azad et al., 2014; Lipplaa et al., 2019). However, the use of these treatments can inhibit physiological bone remodeling and increase the risk of osteonecrotic lesions (Lipplaa et al., 2019). Accordingly, an improved understanding of CD301-mediated cell fusion could provide a selective treatment for IL-4-driven MGC-containing disease processes.

In conclusion, IL-4-induced MGC formation is evidently dependent on the expression of Mgl2 (in mouse) or CD301 (in human) in macrophages. In contrast, RANKL-induced formation of osteoclasts is independent of CD301. Notably, CD301 appears to be involved in the later stages of cell fusion events, which lead to the generation of MGCs with large numbers of nuclei. Further investigations into MGCs with broader CD301 expression profiles may show that this protein is a phenotypic marker of reactionary/reparative processes. These findings could rationalize its use as a diagnostic and therapeutic target of MGC-containing lesions.

MATERIALS AND METHODS

Primary bone marrow monocyte isolation

All procedures were performed in accordance with the Guide for the Humane Use and Care of Laboratory Animals, and were approved by the University of Toronto Animal Care Committee. Bone marrow was harvested from tibia and femurs of male C57BL/6 mice between 6 and 10 weeks old. Single-cell suspensions were prepared from marrow in complete minimum essential medium alpha (αMEM), which includes 10% fetal bovine serum and 164 IU/ml of penicillin G, 50 mg/ml of gentamicin and 0.25 mg/ml of fungizone. Cells were added to T-75 cm^2 flasks (10^6 cells/ml), incubated overnight, then centrifuged over Ficoll-Paque Plus, at 300 ***g*** for 30 min at room temperature, washed with αMEM, then plated at 10^5 cells/ml with M-CSF (20 ng/ml) for 4 days before experimentation.

Cell culture

RAW264.7 and THP-1 cells from ATCC were cultured in complete Dulbecco's modified Eagle's medium (DMEM) or Roswell Park Memorial Institute medium with 0.05 mM β-mercaptoethanol), respectively. Cellular phenotype was examined at each subculture; pleuropneumonia-like organism infection was examined by DAPI staining at every subculture and there was no evidence of infection. Complete medium was medium that was supplemented with 10% fetal bovine serum, 164 IU/ml penicillin G, 50 µg/ml gentamicin and 0.25 µg/ml fungizone. Medium and cytokines were replenished every 48 h during experiments. Cells were seeded in 60 mm^2 culture dishes at 5×10^6 cells/dish.

TMT-MS

Mouse macrophage RAW264.7 cells were treated with RANKL (60 ng/ml), IL-1β (20 ng/ml), IL-4 (10 ng/ml) or TNF (10 ng/ml), fixed on day 5 of culture with 4% paraformaldehyde (PFA), washed with PBS, and frozen. Relative protein quantification was determined with TMT-MS using stable isotopic labels, and a comparison of peptide counts from proteins that were identified with high probability (P<0.05). Samples were fractionated into three groups, allowing for one missed cleavage. Data were analyzed with Scaffold Q+ software. Relative abundances of $\log_2$ fold change (more than 0.5 or less than −0.5) were tabulated (overexpressed and underexpressed, respectively). Data from these experiments will be made accessible by request to the corresponding author (C.A.M.).

Fusion assays

RAW264.7 cells were plated at 10,000 cells per well on fibronectin-coated eight-well chamber slides with complete DMEM and with vehicle-only

Journal of Cell Science (2020) 133, jcs248864. doi:10.1242/jcs.248864

treatment or IL-4 (10 ng/ml) for 6 days. Rat anti-mouse CD301 IgG2a monoclonal antibody (ER-MP23; 50 µg/ml, Novus Biologicals) or its isotype control (50 µg/ml, BioLegend rat IgG2a, RTK2758) were added to wells directly for antibody inhibition experiments. Medium, antibodies and cytokines were replenished every 48 h. The authenticity of the blocking antibody was assessed by comparison with the isotype control and its lack of efficacy in blocking in cells that did not express CD301.

In some experiments, primary mouse monocytes were plated in complete αMEM and with either recombinant mouse M-CSF or granulocyte M-CSF (GM-CSF) (20 ng/ml). In experiments that examined the effect of certain cytokines on the expression of CD301, the following cytokines were added to culture medium at the indicated concentrations: RANKL (60 ng/ml), LPS (10 ng/ml), INFγ (1 ng/ml), IL-1β (20 ng/ml), TNF (10 ng/ml), IL-4 (10 ng/ml) or TGF-β1 (5 ng/ml).

In experiments that examined the role of CD301 in human monocyte fusion, human monocytic THP-1 cells were plated as described above, with the addition of recombinant hM-CSF (20 ng/ml) alone, or with RANKL (60 ng/ml) or recombinant human IL-4 (10 ng/ml). For experiments in which CD301 activation or inhibition experiments were conducted using THP-1 cells, N-acetylgalactosamine (GalNAc; α-GalNAc-PAA-biotin, GlycoTech, 1 µg/ml) or recombinant human CD301 (R&D Systems, 4888-CL, 1 µg/ml) were added and replenished with the indicated cytokines. Full-length recombinant CD301 (from R&D Systems) forms trimers in solution, which enables binding to glycans and, as a result, inhibits activation of membrane-bound CD301 (Beatson et al., 2015; Jégouzo et al., 2013). After 6 days, all cells were fixed with PFA for 20 min, washed with PBS, stained with Alexa Fluor 488 Phalloidin (for actin filaments) at room temperature for 20 min, stained with DAPI (for nuclei) for 10 min, mounted and imaged by confocal microscopy. Cells were considered to have fused if there were three or more nuclei per cell. The number of fused nuclei was divided by the total nuclei and expressed as a percentage.

Relationship of CD301 with the plasma membrane

For studying the spatial relationship between CD301 and the plasma membrane, we used membrane labeling with concanavalin A, which was followed by immunostaining with CD301. Briefly, RAW264.7 cells (10^4 cells/well, passage 8) were incubated in 700 µl complete DMEM with or without recombinant murine IL-4 (PeproTech, 214-14, 10 ng/ml) in eight-well chamber slides (Falcon) for 4 days. Cell culture medium was changed at day 2. The medium was removed and cells were rinsed with prewarmed Hank's Balanced Salt Solution (HBSS, Wisent Bioproducts, 311-515-CL). Live cells were stained with HBSS (250 µl/well) containing 50 µg/ml concanavalin A-Alexa Fluor 594 (Invitrogen, C11253) at 37°C for 30 min. The cells were washed with HBSS and fixed with 4% PFA in PBS for 20 min. After being washed three times with PBS, the fixative was quenched with 100 mM glycine in PBS (pH 7.4) for 10 min. Cells were permeabilized with 0.1% Triton X-100 in PBS for 3 min and blocked with 1% bovine serum albumin (BSA) in PBS for 30 min in the dark at room temperature. Cells were incubated with rat anti-mouse CD301 antibody (Novus Biologicals, NB100-64874, 1:500) in 1% BSA/PBS overnight at 4°C. After washing with PBS, cells were stained with goat anti-rat IgG Alexa Fluor 488 (Invitrogen, A-11006, 1:1000 in 1% BSA/PBS) at 37°C for 1 h. Finally, cells were counterstained with DAPI (0.165 µM in PBS, Sigma-Aldrich) for 10 min and imaged by confocal microscopy. Analysis of co-localization of concanavalin A and CD301 was performed using the ImageJ Coloc 2 plug-in for Pearson's correlation coefficient, as described previously (Bolte and Cordelières, 2006).

A second approach was used to examine the relationship between the plasma membrane and CD301. In this instance, plasma membrane proteins were isolated using magnetic beads and immobilized concanavalin A (Lee et al., 2008). Briefly, streptavidin magnetic beads (MJS BioLynx, VECTM1003010), in a 150 µl suspension, were placed into a 1.5 ml Eppendorf tube. Beads were separated from the solution by holding the tube near a magnet; the remnant solution was discarded by pipetting. Beads were washed twice with 1 ml of distilled water, followed by 1 ml of Tris-buffered saline (TBS) containing 150 mM NaCl and 50 mM Tris HCl, pH 7.4. Beads were re-suspended in 245 µl TBS, and 35 µl biotinylated concanavalin A (5 mg/ml, BioLynx, VECTB1005) was added. This suspension was mixed on a rocker for 1 h to enable the binding of biotinylated concanavalin A to streptavidin. Beads were washed sequentially with 1 ml of TBS, 1 ml of TBS with 1% Triton X-100, and three times with 1 ml of TBS. Beads were resuspended in 450 µl of TBS and stored at 4°C. Subsequently, RAW264.7 cells (0.5×10^6/dish, passage 8) were treated with or without IL-4 (10 ng/ml) for 4 days in five 10 cm^2 plates in complete DMEM (10 ml/dish). The medium was changed at day 2. After washing twice with TBS, cells were collected by scraping each plate with 1 ml of TBS. Scraped cell suspensions were collected in a 12 ml centrifuge tube and centrifuged at 325 ***g*** for 5 min to collect the cells. The supernatant was removed and the cell pellet was saved. The pellet was resuspended in 0.5 ml of TBS and homogenized in a 2 ml Dounce homogenizer. An aliquot of the homogenized total cell lysate [50 µl, diluted in 300 µl radioimmunoprecipitation assay (RIPA) buffer] was saved for later analysis. The remaining lysate (in TBS) was added to the streptavidin magnetic beads that had been prepared 1 day before, as described above, and then mixed on a rocker for 1 h. After binding, the streptavidin magnetic beads were collected by holding the tube near a magnet. The unbound flow-through fraction was also saved. Beads were washed with 1 ml of TBS (five times), and proteins that bound to the concanavalin A magnetic beads were eluted with 250 µl TBS containing 0.25 M methyl α-D-mannoside (BioLynx, VECTS9005) and 0.5% 3-[(3-cholamidopropyl)dimethylammonio]-1-propanesulfonate (CHAPS, Sigma-Aldrich). Protein concentrations were measured with a bicinchoninic acid (BCA) kit (Thermo Scientific). Equal amounts of protein samples (20 µg/lane) were run on a 12% SDS polyacrylamide gel for CD301 and for beta-actin. A 7% gel was used to resolve Na^+-K^+ ATPase (a plasma membrane protein), which was followed by immunoblotting. For analyses, goat anti-mouse Mgl2/CD301b antibody from R&D Systems (A2835, 1:200 dilution of 0.2 mg/ml), mouse monoclonal anti-β-actin antibody from Sigma-Aldrich (clone AC-15, A5441, 1:8000), and rabbit anti-α1 Na^+-K^+ ATPase antibody from Cell Signaling Technology (3010, 1:1000) were used. Proteins were visualized using the following secondary antibodies: IRDye 800CW donkey anti-goat IgG, IRDye 680CW goat anti-mouse IgG, or IRDye 800CW goat anti-rabbit IgG, respectively, and a Li-Cor Odyssey detection system.

CRISPR/Cas9-mediated genome editing

Mgl1 KO and Mgl2 KO RAW264.7 cell lines were generated. Mgl1 and Mgl2 DKO RAW264.7 cell lines were also generated with sequential KO of Mgl1 from an Mgl2 KO cell line by Applied StemCell. Two guide RNAs (gRNAs) were chosen for each gene: g1 5′-ACGAAAACCTCCAGAACTCA-3′ and g2 5′-CCTCCAGAACTCAAGGATCG-3′ targeting exon 2 of mouse Mgl1; and g1 5′-AAACTTCCAGAACTTGGAGC-3′ and g2 5′-GGAGCGGGAAGAGAAAAACC-3′ targeting exon 2 of mouse Mgl2 (Fig. S1). Based on endonuclease activity, g2 for Mgl1 and g1 for Mgl2 were chosen, and cloned into a gRNA/Cas9 expression vector and introduced to RAW264.7 cells. Mutagenesis within the targeted regions in a single homozygous cell clone from the transfected cells was identified by PCR (Table S1). Sanger sequencing confirmed multiple clones of Mgl1 KO, Mgl2 KO, and sequentially, Mgl2, then Mgl1 DKO. Two Mgl1 KO clones, A1 (−2, −1 bp) and C1 (−8 bp), and three Mgl2 KO clones, A2 (−2 bp), B3 (−7 bp) and B8 (−17 bp), were analyzed. The Mgl2 KO clone B8 was used for sequential Mgl1 KO; three clones were obtained, G9 (−7 bp), G10 (−56 bp) and F10 (−40 bp). Mgl1 KO clone A1, Mgl2 KO clone B8, and Mgl1/2 double knockout (DKO) clone G10 were utilized for experiments. The growth of selected clones in T-75 flasks was observed over 7 days by phase contrast microscopy.

Re-expression of Mgl2 in Mgl2 KO and Mgl1/2 DKO cell lines

An In-Fusion Cloning kit (Takara) was used for Mgl2 gene cloning and amplification of Myc-DDK-tagged mouse Mgl2 (NM_145137) cDNA (OriGene Technologies), using the primers described in Table S1. The amplified cDNA (2 µg) was inserted into BglII/XhoI-linearized pMSCVpuro and the insertion was confirmed by sequencing. pMSCVpuro-Mgl2-Myc-DDK was co-transfected with pVSV-G into a retroviral packaging cell line GP-293 to produce retrovirus-expressing Mgl2. Mgl2 KO and Mgl1/2 DKO cells were virus infected, and selected

for 2 weeks with 7 µg/ml puromycin and maintained in cell culture medium with 3 µg/ml puromycin.

Flow cytometry

RAW264.7 wild-type and KO cells treated with cytokines were detached from culture dishes using EDTA, and fixed with fresh methanol-free formaldehyde (1.6% final concentration) for 15 min on ice before processing. Cells (5×10^5 cells/tube) were resuspended (50 µl; 5×10^5 cells/tube) in fluorescence-activated cell sorting buffer (1× $HBSS^{-/-}$, 2 mM EDTA, 1% BSA), blocked with mouse IgG (2 µl mg; Sigma-Aldrich) and rat serum (1 µl; Sigma-Aldrich), then labeled with APC-tagged rat anti-mouse Mgl2 antibody (1:50, BioLegend; clone LOM-14; Rat IgG2b, κ). Mgl2 null cells did not show significant staining with this antibody. Sample acquisition was performed using a Sony flow cytometer (Spectral Analyzer). At least 2×10^5 gated events were acquired for each sample. Data were analyzed using FCS Express software (Version 7; De Novo Software).

qPCR

Total RNA was extracted (RNeasy Mini Kit, Qiagen) and residual genomic DNA was digested (RNase-Free DNase Kit, Qiagen). The RNA concentration was determined using a NanoDrop spectrophotometer. RNA quality was analyzed with an Agilent Technologies Bioanalyzer. Total RNA (1 µg) was reverse-transcribed into cDNA using Oligo-dT18 VN primers (ACGT Corp). qRT-PCR was performed in triplicate (Bio-Rad CFX96 real-time system). CFX Manager Software (Version 1.0) was used to analyze PCR results; mRNA expression was normalized to the housekeeping gene GAPDH (Table S1). For detection of CD301 in THP-1 cells, each 20 µl reaction contained 5 µl of 1:10 diluted cDNA, 200 nM of forward and reverse primers and 10 µl of the Advanced qPCR master mix (Wisent). RNA expression was normalized to the housekeeping gene beta-actin. PCR primers used for human CD301 detection were designed using mRNA sequence previously deposited in GenBank (NM_182906.4) (Ostrop et al., 2015).

Western blotting

After 5 days of culture, cells were lysed (RIPA buffer containing protease inhibitors), sedimented and the supernatants were collected. Protein was quantified using a BCA kit; 30 µg of protein in Laemmli sample buffer was boiled for 10 min, separated by 10% SDS-PAGE and transferred to nitrocellulose membranes for 90 min. Membranes were blocked with 5% milk, incubated overnight at 4°C with goat anti-mouse CD301 (Novus Biologicals, AF4888, 1:200) and mouse anti-β-actin (Sigma-Aldrich, A5441, 1:800) antibodies with gentle shaking. The authenticity of the antibody was evaluated through the knockdown experiments described in the Results. Membranes were washed with Tris-buffered saline with 0.2% Tween 20, incubated with secondary antibodies (IRDye 800CW donkey anti-goat IgG and IRDye 680CW goat anti-mouse IgG, both 1:1000) and blot densities quantified (Li-Cor Odyssey). Densitometry analysis was performed using ImageJ software; CD301 was normalized to beta-actin expression.

Immunofluorescence

RAW264.7 cells were plated (100,000 cells/well) on fibronectin-coated eight-well chamber slides with complete DMEM containing vehicle, RANKL (60 ng/ml), IL-1β (20 ng/ml), IL-4 (10 ng/ml) or TNF (10 ng/ml) for 4 days. Medium and cytokines were replenished every 48 h. Cells were fixed with 4% PFA for 20 min, quenched, permeabilized (0.1% Triton X-100 in PBS) and blocked with BSA (1% in PBS containing 0.1% Triton X-100). Cells were incubated with rat anti-mouse CD301 IgG2a monoclonal antibody (1:500, Novus Biologicals) at 4°C overnight, stained with Alexa Fluor 488 goat anti-rat IgG (H+L) antibody (1:500, Invitrogen) at 37°C for 1 h, then Phalloidin-Texas Red-stained, and DAPI stained before mounting and imaging using a Leica SP8 confocal microscope.

Glycan-bead preparation and bead binding assays

Magnetic streptavidin-bound 2.8 µm beads (Invitrogen Dynabeads) were prepared by incubation with biotinylated glycans GalNAc and Sialyl-Lewis X (Le^X) (alpha-GalNAc-PAA-biotin; Le^X-PAA-biotin, GlycoTech; 3:1 ratio); then added to cells directly after washing. Wild-type or KO cells were plated at 50,000 cells/well with complete DMEM with no treatment or IL-4 (10 ng/ml) for 3 days. Medium and cytokines were replenished after 48 h. For antibody inhibition experiments, rat anti-mouse CD301 IgG2a monoclonal antibody (50 µg/ml, Novus Biologicals) or isotype control (50 µg/ml, BioLegend rat IgG2a, RTK2758) were added to the wells 1 h before bead addition. Unbound, GalNAc- or Le^X-bound beads (6.7×10^8 beads/ml) were incubated with cells for 1 h, PFA fixed, washed, then Phalloidin-488- and DAPI-stained. Slides were mounted and imaged using a confocal microscope. The number of beads bound to membranes and unbound beads were counted, and their ratio was expressed as a percentage.

Human biopsies

With approval from the University of Toronto Research Ethics Board (#35822) (which included obtaining appropriate consent), samples of peripheral and central giant cell granulomas were obtained from the Toronto Oral Pathology Service, Faculty of Dentistry, University of Toronto. All clinical investigations were conducted in accord with the principles expressed in the Declaration of Helsinki. Sections (5 µm) from paraffin-embedded biopsy specimens were mounted on glass slides, heated for 30 min at 60°C, antigen retrieved (citrate buffer, pH 6.0, Abcam), H_2O washed, permeabilized (Triton X-100), blocked (Sea Block Serum, Abcam), immunostained with mouse monoclonal anti-human CD68 Alexa Fluor 405 (Novus Biologicals, NB600-985AF405, 1:200) and mouse anti-human CD301 Alexa Fluor 546 (Novus Biologicals, DDX0010A546-100, 1:200), counterstained with DRAQ7 (Abcam, ab109202, 3 µM), imaged using a confocal microscope on the same day, and analyzed using Volocity 3D Image Analysis Software (PerkinElmer). Normal human oral mucosa and liver paraffin sections (Amsbio, HP-314) were likewise stained as CD301-negative and positive controls, respectively.

Statistical analysis

Mean and s.e.m. were calculated for all continuous variables. An unpaired Student's *t*-test was used for comparisons of two samples; one- and two-way ANOVA analyses with Tukey's post-hoc test were employed for analysis of multiple samples. Numerical data are expressed as mean±s.e.m., and for all experiments, each experiment was repeated on different days at least in triplicate and in some instances up to six trials, with each experiment comprising a minimum of three separate culture dishes. For TMT-MS, duplicate assays were performed. For all analyses employing flow cytometry, a minimum of 10,000 events were analysed. Statistical significance is indicated as $*P<0.05$, $**P<0.01$, $***P<0.001$, and $****P<0.0001$. We found in initial experiments that with sample sizes of a minimum of three separate experiments conducted on different days, and with each experiment containing a minimum of three samples, that our ability to detect statistically significant differences ($P<0.05$) was not affected by insufficient power.

Acknowledgements

We are grateful to Dhaarmini Rajshanhkar, Wilson Lee and Aiman Ali for technical support with imaging and immunostaining optimization. We are particularly grateful to Grace Bradley and the University of Toronto Oral Pathology Service for the selection and provision of human biopsy specimens.

Competing interests

The authors declare no competing or financial interests.

Author contributions

Conceptualization: P.J.B., M.G., C.A.M.; Methodology: P.J.B., Y.W., M.A.M., C.A.M.; Validation: P.J.B., Y.W., M.A.M., C.A.M.; Formal analysis: P.J.B., Y.W., M.A.M., C.A.M.; Investigation: P.J.B., C.A.M.; Resources: Y.W., C.A.M.; Data curation: P.J.B., C.A.M.; Writing - original draft: P.J.B., C.A.M.; Writing - review & editing: P.J.B., Y.W., C.A.M.; Visualization: P.J.B., Y.W.; Supervision: C.A.M.; Project administration: M.G., C.A.M.; Funding acquisition: M.G., C.A.M.

Funding

P.J.B. was supported by funding from a Queen Elizabeth II Graduate Scholarship in Science and Technology and Ontario Graduate Scholarships. C.A.M. is supported by a Canada Research Chair (Tier 1) in Matrix Dynamics. The research was

funded by Canadian Institutes of Health Research (CIHR) grant MOP-142250 to M.G. and C.A.M., and an Alpha Omega Foundation of Canada Grant.

Supplementary information

Supplementary information available online at
https://jcs.biologists.org/lookup/doi/10.1242/jcs.248864.supplemental

Peer review history

The peer review history is available online at
https://jcs.biologists.org/lookup/doi/10.1242/jcs.248864.reviewer-comments.pdf

References

Azad, A. K., Rajaram, M. V. S. and Schlesinger, L. S. (2014). Exploitation of the macrophage mannose receptor (CD206) in infectious disease diagnostics and therapeutics. *J. Cytol. Mol. Biol.* **10**, 1.

Beatson, R., Maurstad, G., Picco, G., Arulappu, A., Coleman, J., Wandell, H. H., Clausen, H., Mandel, U., Taylor-Papadimitriou, J., Sletmoen, M. et al. (2015). The breast cancer-associated glycoforms of MUC1, MUC1-Tn and sialyl-Tn, are expressed in COSMC wild-type cells and bind the c-type lectin MGL. *PLoS ONE* **10**, e0125994. doi:10.1371/journal.pone.0125994

Bolte, S. and Cordelières, F. P. (2006). A guided tour into subcellular colocalization analysis in light microscopy. *J. Microsc.* **224**, 213-232. doi:10.1111/j.1365-2818.2006.01706.x

Denda-Nagai, K., Kubota, N., Tsuiji, M., Kamata, M. and Irimura, T. (2002). Macrophage C-type lectin on bone marrow-derived immature dendritic cells is involved in the internalization of glycosylated antigens. *Glycobiology* **12**, 443-450. doi:10.1093/glycob/cwf061

Denda-Nagai, K., Aida, S., Saba, K., Suzuki, K., Moriyama, S., Oo-Puthinan, S., Tsuiji, M., Morikawa, A., Kumamoto, Y., Sugiura, D. et al. (2010). Distribution and function of macrophage galactose-type C-type lectin 2 (MGL2/CD301b): efficient uptake and presentation of glycosylated antigens by dendritic cells. *J. Biol. Chem.* **285**, 19193-19204. doi:10.1074/jbc.M110.113613

Gupta, S., Narwal, A., Kamboj, M., Devi, A. and Hooda, A. (2019). Giant cell granulomas of jaws: a clinicopathologic study. *J. Oral Maxillofac. Res.* **10**, e5. doi:10.5037/jomr.2019.10205

Helming, L. and Gordon, S. (2009). Molecular mediators of macrophage fusion. *Trends Cell Biol.* **19**, 514-522. doi:10.1016/j.tcb.2009.07.005

Higashi, N., Morikawa, A., Fujioka, K., Fujita, Y., Sano, Y., Miyata-Takeuchi, M., Suzuki, N. and Irimura, T. (2002). Human macrophage lectin specific for galactose/N-acetylgalactosamine is a marker for cells at an intermediate stage in their differentiation from monocytes into macrophages. *Int. Immunol.* **14**, 545-554. doi:10.1093/intimm/dxf021

Jégouzo, S. A. F., Quintero-Martínez, A., Ouyang, X., dos Santos, Á., Taylor, M. E. and Drickamer, K. (2013). Organization of the extracellular portion of the macrophage galactose receptor: a trimeric cluster of simple binding sites for N-acetylgalactosamine. *Glycobiology* **23**, 853-864. doi:10.1093/glycob/cwt022

Kumar, V., Abbas, A. K. and Aster, J. C. (2015). *Robbins and Cotran Pathological Basis of Disease*, 9th edn. Philadelphia, Pennsylvania: Elsevier.

Lee, Y.-C., Block, G., Chen, H., Folch-Puy, E., Foronjy, R., Jalili, R., Jendresen, C. B., Kimura, M., Kraft, E., Lindemose, S. et al. (2008). One-step isolation of plasma membrane proteins using magnetic beads with immobilized concanavalin A. *Protein Expr. Purif.* **62**, 223-229. doi:10.1016/j.pep.2008.08.003

Lipplaa, A., Dijkstra, S. and Gelderblom, H. (2019). Challenges of denosumab in giant cell tumor of bone, and other giant cell-rich tumors of bone. *Curr. Opin. Oncol.* **31**, 329-335. doi:10.1097/CCO.0000000000000529

Lu, J., Cao, Q., Zheng, D., Sun, Y., Wang, C., Yu, X., Wang, Y., Lee, V. W., Zheng, G., Tan, T. K. et al. (2013). Discrete functions of M2a and M2c macrophage subsets determine their relative efficacy in treating chronic kidney disease. *Kidney Int.* **84**, 745-755. doi:10.1038/ki.2013.135

MacMicking, J., Xie, Q.-W. and Nathan, C. (1997). Nitric oxide and macrophage function. *Annu. Rev. Immunol.* **15**, 323-350. doi:10.1146/annurev.immunol.15.1.323

McNally, A. K. and Anderson, J. M. (1995). Interleukin-4 induces foreign body giant cells from human mono-cytes/macrophages: Differential lymphokine regulation of macrophage fusion leads to morphological variants of multinucleated giant cells. *Am. J. Pathol.* **147**, 1487-1499.

McNally, A. K. and Anderson, J. M. (2011). Macrophage fusion and multinucleated giant cells of inflammation. *Adv. Exp. Med. Biol.* **713**, 97-111. doi:10.1007/978-94-007-0763-4_7

McNally, A. K., DeFife, K. M. and Anderson, J. M. (1996). Interleukin-4-induced macrophage fusion is prevented by inhibitors of mannose receptor activity. *Am. J. Pathol.* **149**, 975-985.

Mendoza, M. C., Vilela, M., Juarez, J. E., Blenis, J. and Danuser, G. (2015). ERK reinforces actin polymerization to power persistent edge protrusion during motility. *Sci. Signal.* **8**, ra47. doi:10.1126/scisignal.aaa8859

Mills, C. D., Kincaid, K., Alt, J. M., Heilman, M. J. and Hill, A. M. (2000). M-1/M-2 macrophages and the Th1/Th2 paradigm. *J. Immunol.* **164**, 6166-6173. doi:10.4049/jimmunol.164.12.6166

Morishima, S., Morita, I., Tokushima, T., Kawashima, H., Miyasaka, M., Omura, K. and Murota, S. (2003). Expression and role of mannose receptor/terminal high-mannose type oligosaccharide on osteoclast precursors during osteoclast formation. *J. Endocrinol.* **176**, 285-292. doi:10.1677/joe.0.1760285

Mosser, D. M. and Edwards, J. P. (2008). Exploring the full spectrum of macrophage activation. *Nat. Rev. Immunol.* **8**, 958-969. doi:10.1038/nri2448

Neville, B. W., Damm, D. D., Allen, C. M. and Chi, A. C. (2016). *Oral and Maxillofacial Pathology*, 4th edn. St. Louis, Missouri: Elsevier.

Ostrop, J., Jozefowski, K., Zimmermann, S., Hofmann, K., Strasser, E., Lepenies, B. and Lang, R. (2015). Contribution of MINCLE-SYK signaling to activation of primary human APCs by mycobacterial cord factor and the novel adjuvant TDB. *J. Immunol.* **195**, 2417-2428. doi:10.4049/jimmunol.1500102

Raes, G., Brys, L., Dahal, B. K., Brandt, J., Grooten, J., Brombacher, F., Vanham, G., Noël, W., Bogaert, P., Boonefaes, T. et al. (2005). Macrophage galactose-type C-type lectins as novel markers for alternatively activated macrophages elicited by parasitic infections and allergic airway inflammation. *J. Leukoc. Biol.* **77**, 321-327. doi:10.1189/jlb.0304212

Sens, K. L., Zhang, S., Jin, P., Duan, R., Zhang, G., Luo, F., Parachini, L. and Chen, E. H. (2010). An invasive podosome-like structure promotes fusion pore formation during myoblast fusion. *J. Cell Biol.* **191**, 1013-1027. doi:10.1083/jcb.201006006

Singh, S. K., Streng-Ouwehand, I., Litjens, M., Weelij, D. R., García-Vallejo, J. J., van Vliet, S. J., Saeland, E. and van Kooyk, Y. (2009). Characterization of murine MGL1 and MGL2 C-type lectins: distinct glycan specificities and tumor binding properties. *Mol. Immunol.* **46**, 1240-1249. doi:10.1016/j.molimm.2008.11.021

Souza, P. E. A., Gomez, R. S., Xavier, G. M., Coelho dos Santos, J. S., Gollob, K. J. and Dutra, W. O. (2005). Systemic leukocyte activation in patients with central giant cell lesions. *J. Oral Pathol. Med.* **34**, 312-317. doi:10.1111/j.1600-0714.2004.00276.x

Syrio, N. F. L., Faria, D. R., Gomez, R. S., Gollob, K. J., Dutra, W. O. and Souza, P. E. A. (2011). IL-10 and IL-10 receptor overexpression in oral giant cell lesions. *Med. Oral Patol Oral Cir. Bucal* **16**, e488-e492. doi:10.4317/medoral.16.e488

Takahashi, N., Yamana, H., Yoshiki, S., Roodman, G., Mundy, G., Jones, S., Boyde, A. and Suda, T. (1988). Osteoclast-like cell formation and its regulation by osteotropic hormones in mouse bone marrow cultures. *Endocrinology* **122**, 1373-1382. doi:10.1210/endo-122-4-1373

van Vliet, S. J., Gringhuis, S. I., Geijtenbeek, T. B. H. and van Kooyk, Y. (2006). Regulation of effector T cells by antigen presenting cells via interaction of the C-type lectin MGL with CD45. *Nat. Immunol.* **7**, 1200-1208. doi:10.1038/ni1390

van Vliet, S. J., Bay, S., Vuist, I. M., Kalay, H., García-Vallejo, J. J., Leclerc, C. and van Kooyk, Y. (2013). MGL signaling augments TLR2-mediated responses for enhanced IL-10 and TNF-α secretion. *J. Leukocyte Biol.* **94**, 315-323. doi:10.1189/jlb.1012520

Wang, L.-X., Zhang, S.-X., Wu, H.-J., Rong, X.-L. and Guo, J. (2019). M2b macrophage polarization and its roles in diseases. *J. Leukoc. Biol.* **106**, 345-358. doi:10.1002/JLB.3RU1018-378RR

Yagi, M., Miyamoto, T., Sawatani, Y., Iwamoto, K., Hosogane, N., Fujita, N., Morita, K., Ninomiya, K., Suzuki, T., Miyamoto, K. et al. (2005). DC-STAMP is essential for cell-cell fusion in osteoclasts and foreign body giant cells. *J. Exp. Med.* **202**, 345-351. doi:10.1084/jem.20050645

Zelensky, A. N. and Gready, J. E. (2005). The C-type lectin-like domain superfamily. *FEBS J.* **272**, 6179-6217. doi:10.1111/j.1742-4658.2005.05031.x

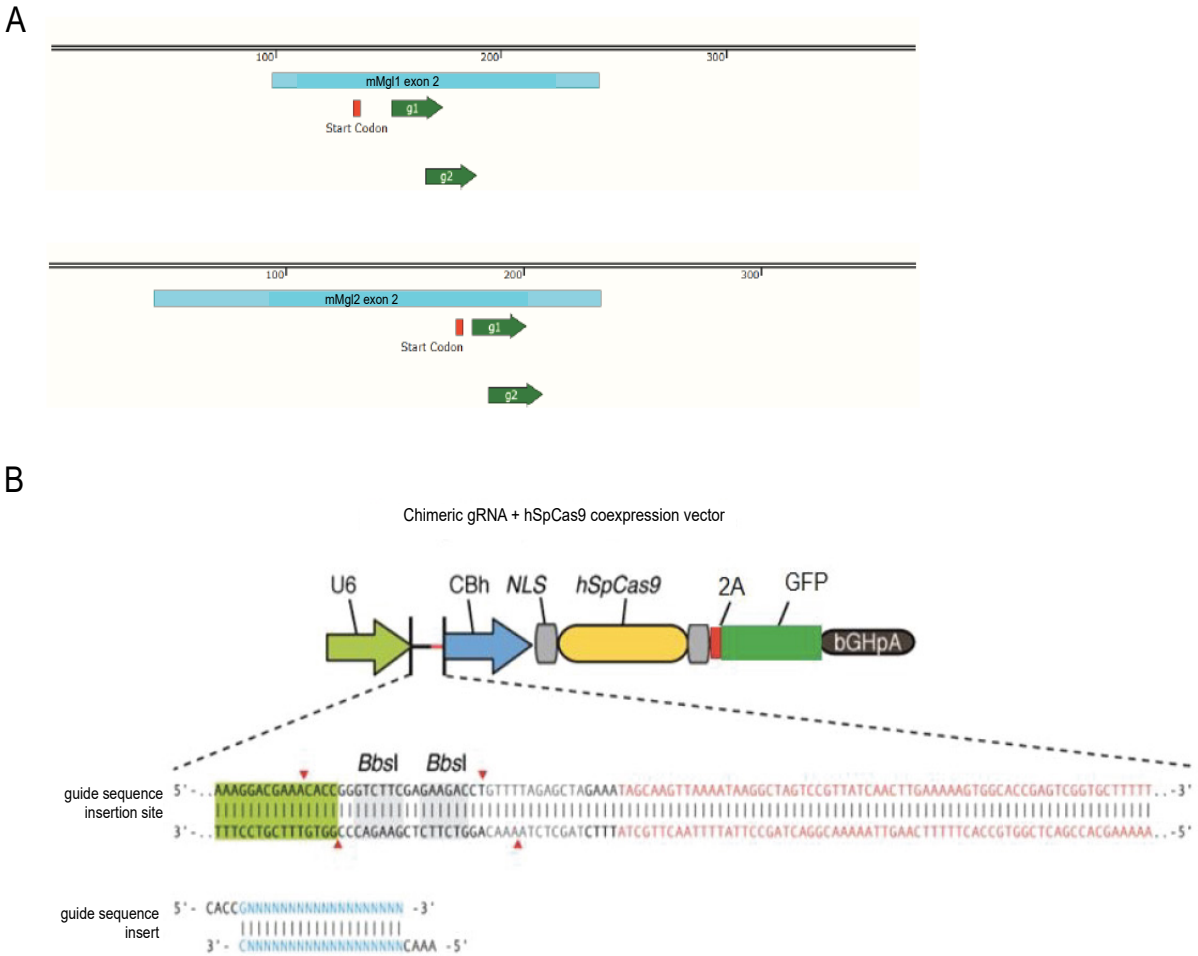

Figure S1. CRISPR/Cas9 target and excise sequences out of the Mgl1 and Mgl2 genes. A) Illustration of the gRNA candidates (green) targeting exon 2 of the both the Mgl gene loci. B) Schematic representation of the gRNA and Cas9 co-expression vector transfected to RAW264.7 cells for assessment of non-homologous end joining (NHEJ) frequencies as indicators of gRNA activity. C) % Normalized NHEJ of Mgl1 g1 and g2, and Mgl2 g1 and g2 guide RNA using next generation sequencing (NGA) show sufficient activity of Mgl1 g1 and g2 as well as Mgl2 g1.

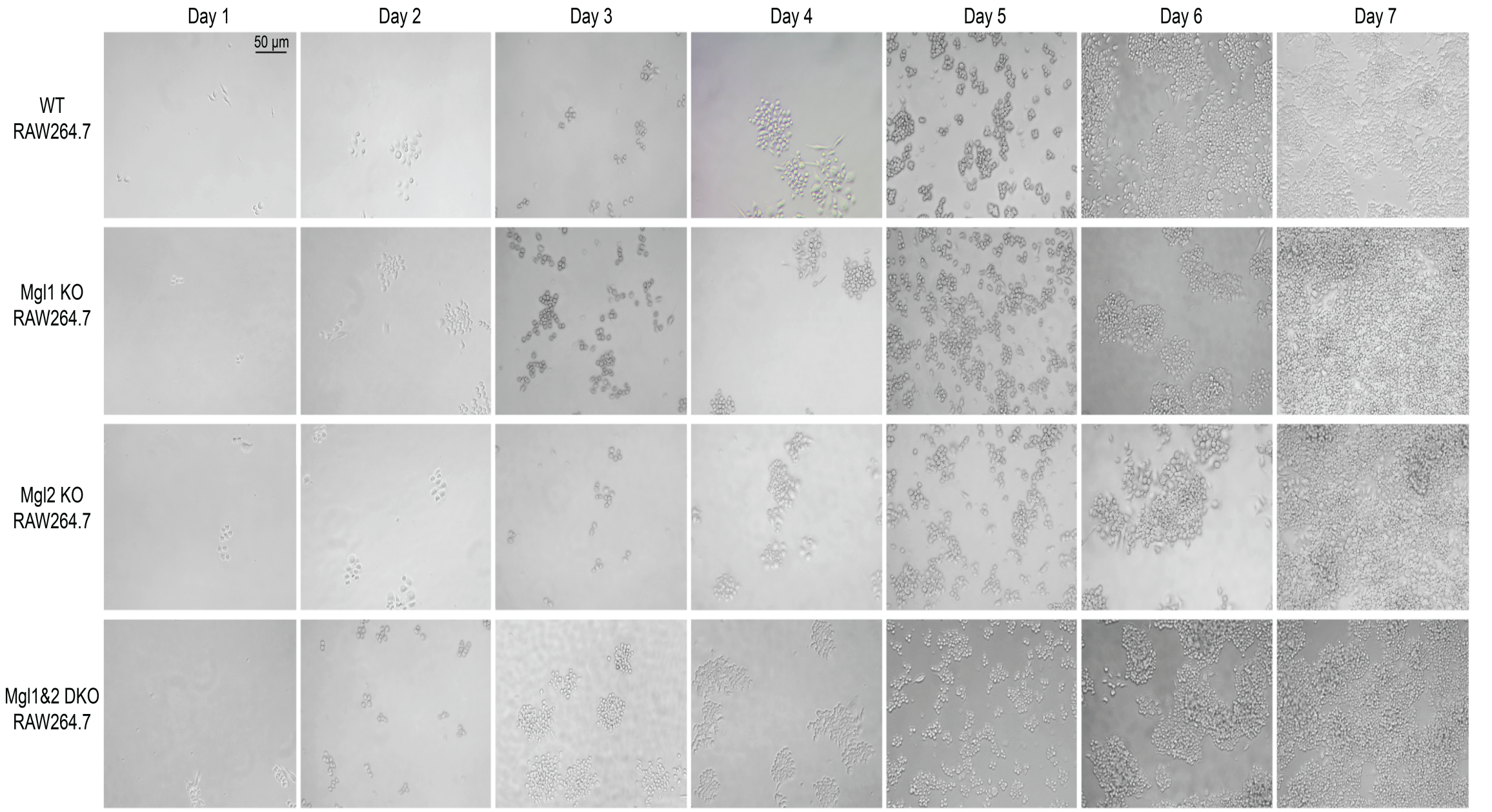

Figure S2. WT, Mgl1 and Mgl2 Knockout (KO), and Mgl1&2 Double KO (DKO) RAW264.7 cell adherence, viability and cell growth. WT, Mgl1 KO, Mgl2 KO, and DKO cells were cultured in complete DMEM in T-75 flasks plated at 1x 10^4 cells/mL with the media replenished every three days. Cells were imaged daily using a Zeiss Primo Vert light microscope for seven days.

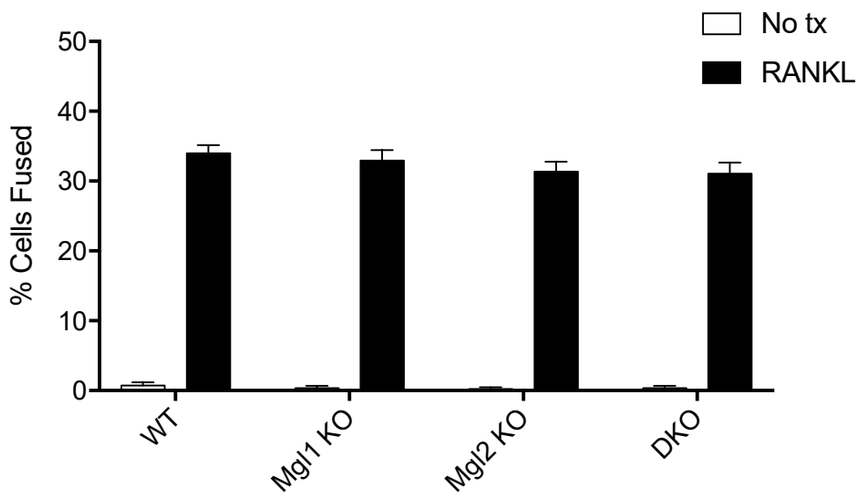

Figure S3. RANKL-induced fusion events in WT and KO cells. WT, Mgl1 KO, Mgl2 KO, and DKO cells were cultured with and without RANKL for 6 days. Cells were fixed, stained with Alexa 488 phalloidin and DAPI. The percentage of cells that had undergone fusion events were quantified.

Table S1. Primers Used for PCR Reactions

Primers for PCR Reactions	
Mgl1 Forward	5'- CAGGCTGCCTCATTCTTGCTCTAAC-3'
Mgl1 Reverse	5'- CTTCACAATGGGTCCTGGGTCC-3'
Mgl2 Forward	5′-GTATTCAACCCCAGCCACAGCC-3′
Mgl2 Reverse	5′-GAATGTGTAATGAGCCTTGGAGTGTACC-3′
Primers for In Fusion Gene Cloning	
Mgl2 Forward	5'-CGCCGGAATTAGATCTCGCCACCATGACAATGAG-3'
Mgl2 Reverse	5'-ATTCGTTAACCTCGAGTCATTAAACCTTATCGTCGTCATCC-3'
Primers for RT-PCR Reactions	
Mgl1&2 Forward	5'-AAGGCAGCTGCTATTGGTTCT-3'
Mgl1-317 Reverse	5'-ATCATCATTCCAGGGACCACC-3'
Mgl2-402 Reverse	5'-CTGAGGCTATAAGTTGTGGGGAG-3'
GAPDH Forward	5'-CCTTCCGTGTTCCTACCCC-3'
GAPDH Reverse	5'-GCCCAAGATGCCCTTCAGT-3'